Fast Estimation of Transverse Fields in High Finesse Optical Cavities

DCC # LIGO-T960140-00-R

Preprint intended for JOSA A.

Partha Saha,

Department of Physics and Center for Space Research,

MIT, Cambridge, MA 02139.

January 15, 1995

revised August 14, 1996.

Abstract

Optical cavities with imperfect geometries have resonant transverse field modes whose spatial descriptions usually deviate from known mathematical functions. Numerical methods are then used to approximate the fields inside the cavities, and we review one method that is in current use by groups designing large interferometric systems for gravitational wave detection. The method suffers from a large increase in computational time as the finesse of the cavity is increased. We present a modified method that cuts down the computational time significantly (by factors of 10 to 100 in the cases we consider) without affecting the accuracy of the results.

Keywords: Optical cavities, high finesse, transverse field modes, numerical methods.

I. Introduction

Design of laser cavities has motivated calculations of transverse optical resonator modes for some time now. Solutions of the free space paraxial propagation equation usually found in textbooks[1] become the transverse modes when two appropriately shaped mirrors — forming a simple optical resonator — reflect, without perturbing, these solutions back and forth into the space between them. When mirrors have more complicated geometries, numerical or perturbative techniques are required.[2−3] Over time, calculations have shifted from using the diffraction integral propagation[2−3] to more numerically efficient Fast Fourier Transform techniques.[4−5]

A related problem is the description of the steady-state transverse field inside an optical cavity when an external laser beam illuminates its mirrors. This is of interest in the design of passive cavities for tasks such as laser frequency stabilization, or more complex ones such as interferometric gravitational wave detection.[6,7] This problem is slightly different from finding the most dominant mode (or the mode with the highest finesse) in a laser cavity: the external beam has to be first projected onto the eigen-modes of the optical cavity, and then each eigen-mode has to be weighted according to its finesse and projection and then summed to form the internal field. In a realistic situation, the optical cavity would deviate from the perfect “textbook” geometry — the mirrors will have surface aberrations and finite size, the alignment will not be perfect, and the external beam will have been corrupted from its transverse laser cavity mode by optics in its path. Current gravitational wave detection schemes[7,8] require the design of a large and expensive interferometric system – and, since such systems are not already in existence anywhere, have to rely on careful and accurate modeling on a computer. This poses no fundamental problems, as the relevant issues and basic physics are already well understood from years of experience with smaller interferometer proto-types. What is needed is to capture the knowledge in a computer tool that can accurately and reliably allow the designer to incorporate all realistic “defects” in evaluating his design. To get the information out to the designer as efficiently as possible, the techniques used in the computer tool deserve attention: it is clear that calculation of eigen-modes for every case is tedious, and sometimes, with finite mirrors, quite challenging. A numerical method that closely follows the actual dynamics of the internal field reaching a steady-state is thus preferred. However, the drawback of such an approach is obvious: what takes place at the speed of light in nature needs to be calculated with the speed of our best computers.

Exactly such a method for estimating the steady-state fields in passive cavities, based on Fast Fourier Transform propagation, has recently been described by Vinet, Hello, Man, and Brillet (henceforth referred to as the method of Vinet and Hello)[9], and also by Trigdell, McClelland, and Savage[10]. Their algorithm is direct, as it iterates on an initial guess for the field and stops when it *converges* to the steady-state one. The method is general, in that the algorithm works without concern for the nature and number of defects, or the description of the external beam. Of course, the answer is valid as long as light propagation, under such circumstances, does not violate the paraxial approximation. Relying on mathematical operations that usually come customized in scientific library subroutines on most computing platforms, the method is easy to implement and package into a useful design tool. However, as could be expected, the method takes many iterations to reach the steady-state field in cavities of high finesse. The purpose of this paper is to present a solution to this problem: to present a fast technique for obtaining steady-state fields inside optical cavities of high finesse (or, equivalently, low loss).

II. Formulation of the steady-state field equation

We deal in this paper with transverse fields, by which we refer to the spatial distribution of the electric field in a plane normal to the direction of propagation. We do not consider changes in the polarization of the field in the optical configurations we consider here, hence the field can be written as a scalar complex function of the coordinates of the transverse plane.

In this section, our aim is to state the problem of finding the steady-state fields inside an illuminated optical cavity as an equation for one unknown field. We will use the geometry of the optical cavity as shown in Figure 1 for setting up the problem. Examining the left 'input' mirror and choosing the sign for the field reflectivity of the interface between air and mirror coating to be negative, the incident fields, E_x and E_b, and the ones leaving it, E_r and E_f, must obey:

$$E_r = t_1 E_b + r_1 E_x, \tag{1}$$

$$E_f = t_1 E_x - r_1 E_b. \tag{2}$$

Here t_1 and r_1 are the transmission and reflectivity of the mirror for the electric field. For mirrors with no loss, $|r|^2 + |t|^2 = 1$. The right hand 'back' mirror in Figure 1 similarly stipulates:

$$E'_r = t_2 E'_f + r_2 E'_x, \tag{3}$$

$$E'_b = t_2 E'_x - r_2 E'_f. \tag{4}$$

For this formulation, let us assume that E'_x and t_2 are 0. Equations 3 and 4 now simplify to $E'_b = -r_2 E'_f$. For the curved back mirror, r_2 is a complex function in x and y, capturing the change in amplitude and phase of the field reflecting off the mirror surface. We will assume in what follows that light incurs negligible loss in power on reflection from this mirror, or that $|r_2| = 1$.

The field E'_f, as shown in the figure, is E_f after propagation in space over the length L of the cavity. This may be expressed, assuming paraxial propagation, as:[1]

$$E'_f(x, y) = \mathbf{FT^{-1}}_{[xy]}[\exp(-ikL + i\frac{(k_x^2 + k_y^2)L}{2k}) \times \mathbf{FT}_{[k_x k_y]}[E_f(x, y)]] \tag{5}$$

In the above equation, λ is the wavelength of light, $\mathbf{FT}_{[k_x k_y]}[\mathcal{E}]$ represents the 2-dimensional Fourier Transform of the field $\mathcal{E}$ resulting in a function in k_x and k_y, and $k = 2\pi/\lambda$. We notice that free space propagation mainly involves the change in phase of the Fourier amplitudes at the different spatial frequencies (k_x, k_y).

We will represent free space propagation over a length L by the action of an operator $\mathbf{K}(z = L)$ or simply $\mathbf{K}$, $E'_f = \mathbf{K}E_f$. It should be clear from Figure 1 that E_b is related to E'_b in exactly the same way — i.e. via a free space propagation over distance L: $E_b = \mathbf{K}E'_b$. Since $E'_b = -r_2 E'_f$, we have $E_b = -\mathbf{K}r_2\mathbf{K}E_f$. Now Equation 2 can be written as

$$E_f = t_1 E_x + r_1 \mathbf{K} r_2 \mathbf{K} E_f. \tag{6}$$

This is the steady-state field equation. Observe that E_f occurs on both sides of the equation and is the unknown field while E_x is the external field whose description is given to us. If we can solve Equation 6 for $E_f(x, y)$, the spatial descriptions of the other fields easily follow from Equations 1, 2 and 5. $E_f(x, y)$ will dynamically relax to this solution in an actual physical situation through many intermediate spatial states. However, once in this state, no further change will take place as long as all the spatial constraints (stated as Equations 1,2, and 5) are satisfied — it is in this sense that E_f in Equation 6 is the spatial steady-state field.

III. Solving for steady-state

In order to make our work useful to the optical designer, we will look at the process of solving the steady-state equation from his perspective, as he is faced with the problem that originally motivated this work. A mirror manufacturer describes the quality of his or her best mirrors by representative mirror maps: e.g., the quality of the surface may be described by the deviation of the surface from the perfect geometry desired, on every point of some 2 dimensional sampling grid. The person designing a gravitational wave detecting interferometer needs to know about the quality of the interference (as expressed through contrast for example) when a laser beam is split equally, reflected off two optical cavities formed with the mirrors, and then brought back and interfered. Accordingly, he may need a computer program that follows the flow diagram shown in Figure 2.

We will attempt to organize the subsequent discussion in this section around all the relevant issues that arise in putting together the code outlined in Figure 2. Optical cavities have some parameters that are nominally chosen and they must enter the steady-state field equation: these include the distance between the two mirrors which is used to form the propagator $\mathbf{K}$, and the reflectivities of the two mirrors which must be used in Equation 6. The alignment and the mirror "defects" need to be incorporated in Equation 6, and we show how to do this in sub-section (a).

Feedback control systems are often used to hold an optical cavity "resonant"; we can define an optical cavity resonant if its length is adjusted such that the internal field strength is maximized. Without any knowledge of the internal field, we can adjust the length of the cavity such that the external beam transmitted into the cavity has no net phase change on a round trip. This is a starting guess; after we actually compute the internal field we may wish to find if its strength is actually at a maximum and adjust the length accordingly. These issues form the basis of discussion in sub-section (c), and constitute steps III and V in the flow of Figure 2.

We then try to approximate a solution to the steady-state equation — in step IV of Figure 2, and in sub-section (b) below. We present the method used in the work of Vinet and Hello and try to show how a high finesse results in slowing convergence to the solution as we iterate on our best guess. We also need to have a measure of the error in our approximate solutions, if we are going to compare fields as in the last step of Figure 2; this is discussed in sub-section (d). Through the sub-sections where necessary, we show why a faster convergence to the solution is important for the optical designer and this then motivates the next section.

(a)*Representation of mirror defects:* Assume that the flat mirror's surface deviates from a plane by $f(x,y)$, and that the optical path length through the mirror via transmission changes over its extent by $g(x,y)$ (both these functions have dimensions of length). For the curved mirror, take as a reference the spherical surface given by the specified radius of curvature and describe the variation from this by $b(x,y)$. If all these functions, $f(x,y)$, $b(x,y)$, and $g(x,y)$, are sufficiently small compared to the wavelength of light, we can, with negligible error,[9] write the steady-state equation for the perturbed cavity as:

$$E_f = t_1 \cdot \exp(-ikg(x,y)) \cdot E_x + r_1 \cdot \exp(-2ikf(x,y)) \cdot \mathbf{K} r_2 \cdot \exp(-2ikb(x,y)) \cdot \mathbf{K} E_f. \quad (7)$$

There is one other defect that enters implicitly in the above equation: the finite size of the mirrors. When the electric field is multiplied by the reflectivity function of the mirror (e.g., $r_1 \cdot \exp(-2ikf(x,y))$ above), the part that falls outside the spatial extent of the mirror is multiplied by zero. As indicated in Figure 2, the functions $f(x,y)$, $g(x,y)$, and $b(x,y)$ are meant to be measured from real mirrors and read into the program. For the examples we present in this paper, however, we simulate these defects with well defined functions.

An important issue in representing the mirror defects and fields is the choice of a two dimensional sampling grid. Given the size of typical mirror imperfections and that FFTs need to be performed on the field vectors, the work of Vinet and Hello[9] shows that a 128×128 grid (whose dimensions need to be determined given the size of the beam) results in the best accuracy with double precision numbers.

(b) *Solving for the steady-state field:* Figure 3 visually guides the reader, through a redrawn Figure 1, to the fields we need to solve for the steady-state field. Introducing the symbols, $T \equiv t_1 \cdot \exp(-ikg(x,y))$, $\mathbf{A} \equiv r_1 \cdot \exp(-2ikf(x,y)) \cdot \mathbf{K} r_2 \cdot \exp(-2ikb(x,y)) \cdot \mathbf{K}$, and letting $E \equiv E_f$, Equation 7 becomes

$$\begin{aligned} E &= TE_x + \mathbf{A}E \qquad (8) \\ \text{or,} \qquad (\mathbf{I} \text{ - } \mathbf{A})E &= TE_x, \end{aligned}$$

where $\mathbf{I}$ is the identity operator. Thus we wish to evaluate (with $E_t \equiv TE_x$),

$$E = (\mathbf{I}\text{-}\mathbf{A})^{-1} E_t. \qquad (9)$$

The expansion, $(\mathbf{I}\text{-}\mathbf{A})^{-1} = \mathbf{I} + \mathbf{A} + \mathbf{A}^2 + \cdots$, offers a solution to Equation 9 immediately:

$$E = E_t + \mathbf{A}\ E_t + \mathbf{A}^2 E_t + \cdots. \qquad (10)$$

Let us consider this solution carefully. The effect of $\mathbf{A}$ is mainly a change in phase of the field E_t, and the only significant loss of field strength occurs on reflection through r_1. In high finesse cavities, $r_1 = 1.0 - \epsilon$ where ϵ is small (typically 0.01 in the cases we have considered), hence the above series converges very slowly. However, interestingly, this is exactly the process by which the internal field is built up inside an optical cavity in reality. In the work of Vinet and Hello, the solution is obtained by iterating on an initial guess. This guess, E_0, is usually the solution in the case of an ideal optical cavity without imperfections — the functions $f(x,y)$, $b(x,y)$, and $g(x,y)$ are all 0, and the mirrors are sufficiently large — with the exciting field assumed to be a mode of this cavity:

$$E_0 = \frac{E_t}{1 - r_1 \cdot \exp(i\psi)}. \qquad (11)$$

In the above equation, ψ is the phase E_t accrues in a round-trip of the cavity. The fields tried iteratively are

$$E_{n+1} = \mathbf{A}E_n + E_t. \qquad (12)$$

Equation 8 is solved if for some n, $E_n = E_t + \mathbf{A}E_n$. As the field is estimated numerically, let the error in our approximation be captured through another field Δ. We decide to stop the iterations when the amplitude in the "error" field, $\Delta_n = E_t + \mathbf{A}E_n - E_n = E_{n+1} - E_n$, falls below a certain threshold δ (i.e. $\sqrt{\sum_{ij} (\Delta_n)^*_{ij} (\Delta_n)_{ij}} \equiv \sqrt{\sum \Delta^*_n \Delta_n} \leq \delta$). This threshold is specified by the person running the simulation as his precision of steady state (Figure 2). We see that

$$\begin{aligned}\Delta_n &= E_{n+1} - E_n \qquad (13)\\ &= \mathbf{A}E_n + E_t - \mathbf{A}E_{n-1} - E_t\\ &= \mathbf{A}(E_n - E_{n-1})\\ &= \mathbf{A}\Delta_{n-1}.\end{aligned}$$

If $\delta_n = \sqrt{\sum \Delta_n^* \Delta_n}$, $\delta_n \approx r_1 \delta_{n-1}$. The relation is approximate because there may be additional losses through the finite size of mirrors. What made Equation 10 unsuitable as a solution — the nearness of r_1 to 1 — also leads to convergence at a slow pace. For example, if $r_1 = \sqrt{0.97}$, it would take about 150 iterations to get every factor of 10 reduction in δ_n; if $\delta_0 = 0.1$, 450 iterations are required to reach a δ of 10^{-4}. Every iteration takes the same amount of computational resources, and thus it is easy to estimate given the hardware how expensive in "real" time (as given by a clock on the wall) a run will be. For example, it takes about 0.4 seconds per iteration on a Connection Machine 5 (CM-5)[11] with a 32 processor partition (one of the faster massively parallel supercomputers), and so for the example above, about 3 minutes per convergence are required. While the number of iterations per convergence is a good hardware-independent measure of speed, it is this amount of "real" time spent that motivates faster convergence methods as we will show in the next section.

(c) *Searching for a resonant length:* How many times do we need to evaluate the steady-state field to locate the resonant length as shown in Figure 2? The steady-state field will differ from an exact solution within limits set by δ as shown in the next section, and so it does not make sense to find a maximum field strength to any better accuracy. Efficient general algorithms that search for an optimum to within a desired accuracy range exist: Brent's method for a single variable maxima search[12] needs to find the steady-state field about 6 to 7 times for fixing the cavity length in the case we studied (with a δ of 10^{-4} for the cavity described in Table 1). We start the algorithm with an analytical estimate for the resonant length[9]. We noted that it took about 3 minutes to converge to a precision of 10^{-4} in the steady-state from an approximate initial guess. However, as we narrow our cavity length search to a more and more restricted interval after testing some resonant length estimates, the steady-state field from the immediately preceding convergence run makes a better starting guess over E_0 from Equation 11. In this way, the resonant length can be determined within 10 to 15 minutes on the CM-5.

While this may not still sound too prohibitive, if we considered coupled cavity systems as planned in the interferometric gravitational wave detection schemes, we would require a great deal of supercomputer time. To optimize a function defined over N variables of a N-cavity system, we need at least $N(N+1)$ single variable searches; thus, for a double cavity system, we need $6 \times 15 = 90$ minutes or 1.5 hours of supercomputer time at a minimum. Improved convergence schemes become imperative.

We wish to emphasize the advantage of using an optimization method that does not use any information based on the modes of the optical cavity. Changing the length or alignment of a cavity to maximize the internal field strength constitutes an attempt to make the cavity see the transmitted external beam as its mode of lowest diffractive loss. Usual models for aligned resonant cavities assume the internal steady-state field to be the TEM_{00} mode, with parameters stipulated by the exciting laser beam. However, there are cavity parameters, like the surface distortion of the mirrors, that cannot be changed at "run" time, and thus the incoming external beam cannot be spatially matched in real situations to the resonant mode exactly. If the cavity is such that the "off-resonant" excitations of the other modes, given the precision required, are not negligible compared to the resonant one, a simple minded TEM_{00} estimate will not be accurate. A general numerical method does not suffer from these complications — working without regard to modal descriptions, it can give the field descriptions achieved in reality by exploring the parameter space until it arrives at the maximum — or for that matter any other kind of optimality (as say defined by a servo system) — in the steady-state field. The generality of the numerical method should be thus evident. It should also be apparent that fast convergence to the steady-state field is essential for such an optimization.

Derivatives of quantities defined on the steady-state fields may be necessary for certain definitions of optimum. These may be computed after approximating the steady-state field at two slightly differing values of the parameter to be varied; however, we wish to show that these can also be determined directly from additional convergence runs. For example, consider the derivative of the power in the steady-state field proportional to $\sum E^*E$, with respect to the length of the cavity — a piece of information useful for hunting for the "resonant" cavity length. The propagator $\mathbf{A}$ in Equation 9 captures the length dependence in an exponent: $-ikL + i((k_x^2 + k_y^2)L)/(2k)$ (Equation 5). The second term in the expression is weakly dependent on length changes of the order of wavelengths, as the paraxial approximation requires that $(k_x^2 + k_y^2)/k^2 \ll 1$. Thus we may rewrite Equation 9 (where $z = 0$) as (for changes in length of the order of wavelengths as actuated by a servo system or noise):

$$
\begin{aligned}
E(z) &= (I - \exp(-ikz)\cdot \mathbf{A})^{-1} E_t, && (14)\\
\text{hence,}\qquad \frac{dE(z)}{dz} &= (-ik\exp(-ikz)\cdot \mathbf{A})(\mathbf{I} - \exp(-ikz)\cdot \mathbf{A})^{-2} E_t, && (15)\\
&= (-ik\exp(-ikz)\cdot \mathbf{A})(I - \exp(-ikz)\cdot \mathbf{A})^{-1} E(z),\\
&= (-ik\exp(-ikz)\cdot \mathbf{A}) E_{dz}
\end{aligned}
$$

Observe that E_{dz} is the steady-state field in the cavity if $E(z)$ is taken as the exciting field instead of E_t in a convergence run. The derivative of the power in the cavity field,

$$\begin{aligned} \frac{d\sum E^*E}{dz} &= \sum E^* \frac{dE}{dz} + \sum (\frac{dE}{dz})^* E, \quad (16) \\ &= -ik[\sum E^* \mathbf{A}(z) E_{dz} - \sum (\mathbf{A}(z) E_{dz})^* E], \\ &= Imag\ \ [2k \sum E^* \mathbf{A}(z) E_{dz}]. \end{aligned}$$

If $E(z)$ is a mode of the cavity, E_{dz} is easily calculated and we may forego the convergence process; however, a general purpose design tool must otherwise rely on such a method.

(d) *Accuracy:* As shown in Figure 2, we are interested in comparing fields from a cavity with real mirrors to those of the ideal one. One measure of the difference in the fields is the Michelson contrast defect, obtained by combining the reflected fields from the two cavities: $1-c \equiv (2I_{min})/(I_{max}+I_{min})$, where I_{min} and I_{max} are the minimum and maximum field intensities obtained from interference by varying the overall phase difference between the two fields. For estimating the errors in the computation of these quantities, we must determine the error in the internal field:

$$\begin{aligned} \Delta_n &= E_{n+1} - E_n, \quad (17) \\ &= \mathbf{A}E_n + E_t - E_n, \\ \Rightarrow \quad E_n &= \mathbf{A}E_n + E_t - \Delta_n, \quad (18) \\ \Rightarrow \quad E_n &= (\mathbf{I}\text{-}\mathbf{A})^{-1}E_t - (\mathbf{I}\text{-}\mathbf{A})^{-1}\Delta_n. \end{aligned}$$

As could have been anticipated, the exact error in the field require us to continue the convergence process. We therefore satisfy ourselves with upper-bounds, overestimating this error by assuming that Δ_n is a resonant mode of the cavity, thus:

$$E_n = E - \frac{\Delta_n}{1 - r_1}. \quad (19)$$

Now we find the error in our derived quantities; for example, the fractional error in power, which is useful because it sets bounds for how accurately the power can be maximized as the length of the cavity is varied, is given by:

$$\frac{|\sum E^*E - \sum E_n^* E_n|}{\sum E_n^* E_n} = \frac{|Re\,[2\sum E_n^* \Delta_n]|}{(1-r_1)\sum E_n^* E_n} \leq \frac{2\delta_n}{(1-r_1)\sqrt{\sum E_n^* E_n}}. \quad (20)$$

Similar expressions can be derived for the contrast defect and other quantities defined on the internal field. Once the cavity designer specifies the accuracy he requires in his quantity of interest, he can, through an equation like Equation 20 above, calculate the final δ_n to be stipulated for his run.

IV. An Accelerated Convergence Scheme

Referring back to Equation 9, we see that we need to invert an operator **I - A** to obtain the steady-state field. The operator can be written as a matrix acting on 128×128 fields but that is not very useful, as we have to then keep track of its $128^2 \times 128^2$ elements. Its action is more easily implemented through optimized FFTs as we have done. Hence the traditional matrix inversion methods, like those of Jacobi, Gauss-Seidel, or successive overrelaxation, do not at first glance help us.

However, observe how the method described before (Equation 12) *resembles* an attempt to invert the matrix by the Jacobi method (it is really a splitting method).[13] We immediately try an over-relaxation method; we write (fields as approximated in the previous method have superscripts SR for straight or simple relaxation),

$$\begin{aligned} E^{\mathrm{SR}}_{n+1} &= E_n + (\mathbf{A}E_n + E_t - E_n). && (21)\\ \text{Overrelaxing the error}^{13},\ E_{n+1} &= E_n + \omega_n(\mathbf{A}E_n + E_t - E_n), && (22)\\ &= (1-\omega_n)E_n + \omega_n(\mathbf{A}E_n + E_t),\\ &= a_n E_n + b_n(\mathbf{A}E_n + E_t), \quad \text{more generally},\\ &= a_n E_n + b_n(E^{\mathrm{SR}}_{n+1}). \end{aligned}$$

Our goal above is simple: we wish to use as our new guess the best superposition of the present guess E_n and the successive one tried in the simple relaxation method, E^{SR}_{n+1}.

Allowing a_n and b_n to be complex and using

$$\Delta_n = (\mathbf{A}E_n + E_t) - E_n = E_t - (\mathbf{I} - \mathbf{A})E_n, \tag{23}$$

we can fix these variables by minimizing $\sum \Delta^*_{n+1}\Delta_{n+1}$. Introducing $D_n = (\mathbf{I} - \mathbf{A})E_n$ and $D^{\mathrm{SR}}_{n+1} = (\mathbf{I} - \mathbf{A})E^{\mathrm{SR}}_{n+1}$, the fields that capture the change (difference) in E_n and E^{SR}_{n+1} after a round trip (refer Figure 3), we see that a_n and b_n require the solution of

$$\begin{bmatrix} \sum D^*_n D_n & \sum D^*_n D^{\mathrm{SR}}_{n+1} \\ & \\ \sum (D^{\mathrm{SR}}_{n+1})^* D_n & \sum (D^{\mathrm{SR}}_{n+1})^* D^{\mathrm{SR}}_{n+1} \end{bmatrix} \begin{bmatrix} a_n \\ \\ b_n \end{bmatrix} = \begin{bmatrix} \sum D^*_n E_t \\ \\ \sum (D^{\mathrm{SR}}_{n+1})^* E_t \end{bmatrix}. \tag{24}$$

Finding a_n and b_n add no significant computational overhead, as overlap summations of the type $\sum \mathcal{E}^*\mathcal{E}$ take negligible time compared to a round trip FFT on vector processing platforms.

We will attempt to explain why this method works through a geometrical picture. If we can choose E_n such that $D_n = E_t$, we have solved Equation 9. When we fail with $E_t - D_n = \Delta_n$ in the relaxation method of the earlier section, our next guess E^{SR}_{n+1} attempts to make D^{SR}_{n+1} equal to E_t and falls short by $E_t - D^{\mathrm{SR}}_{n+1} = \Delta^{\mathrm{SR}}_{n+1}$. It would be optimal to use E_t, or some close estimate, as the next D_{n+1} and find the corresponding E_{n+1}. This is exactly what we are doing in the overrelaxation method: we form a plane with D_n and $D_{n+1}^{\rm SR}$ and find a field in this plane which is closest to E_t; i.e., we find the projection of E_t on the D_n-$D_{n+1}^{\rm SR}$ plane. This projection then becomes D_{n+1} from which we calculate E_{n+1}. Figure 4 illustrates the process with vectors representing the electric fields in a 3 dimensional space (the actual space has infinite dimensions).

A few remarks are appropriate here. We should point out that if $b_n = 1$ and $a_n = 0$, we are back to the simple method of convergence; so the overrelaxation method generalizes that technique. Also, it may seem that we need two round trip FFT computations per iteration, as compared to only one in simple relaxation. This is not true — each iteration starts with the fields E_n and D_n, and we can form $\mathbf{A}E_n + E_t = E_t + E_n - D_n$ without any FFT computations. The only round trip FFT evaluations enter in $\mathbf{A}(\mathbf{A}E_n + E_t)$ to create $D_{n+1}^{\rm SR}$. Another point of concern may be that of $D_{n+1}^{\rm SR}$ being linearly dependent on D_n, so that a blind inversion of the 2×2 matrix in Equation 24 would be disastrous. If E_n lies along a mode of the cavity along with E_t, this situation may arise — but this also implies that no further iteration is needed. It is advisable to take advantage of linear system solvers available in most scientific libraries (like the CMSSL[14] on CM-5) that can catch these kinds of pathologies and take appropriate action.

Now we estimate the speed of the overrelaxation algorithm. We can calculate the expression for $\delta_{n+1} = \sqrt{\sum \Delta_{n+1}^* \Delta_{n+1}}$ exactly and compare it to δ_n, but this exercise is not very illuminating. We will approximate δ_{n+1} from the geometrical picture of Figure 4. Consider the almost isosceles triangle OAB with $\Delta_{n+1}^{\rm SR}$ and Δ_n as its two (nearly) equal sides. The length of the line from the apex O of this triangle meeting the base AB at a right angle is an overestimate for δ_{n+1}. With $r_1 \to 1$, we can write,

$$\delta_{n+1} \leq r_1 \cos[\frac{\theta_n}{2}]\delta_n. \qquad (25)$$

We thus observe where the algorithm receives its boost: from the angle between Δ_n and $\mathbf{A}\Delta_n$. The field Δ_n picks up a part orthogonal to itself on a round trip and help in bringing the error down.

We turn to examples of how much faster the overrelaxation method can be — given some typical cavity defects — in Table 1. The increase in speed ranges from factors of 11 to 175; we could reduce a 15 minute convergence run to a mere 1 minute or less! We compare accuracies of the straight relaxation method to that obtained from overrelaxation in the last column. For this, we first converged to a field E_{ref} by straight relaxation with a δ of 10^{-8}. Next, we compared this field with the E we compute by the two methods with a tolerance δ of 10^{-4}: $E_{err} = E - E_{ref}$. The numbers we show in the column are $(\sqrt{\sum E_{err}^* E_{err}}) \div (\sqrt{\sum E_{ref}^* E_{ref}})$. We should observe that the accuracy is not compromised in the overrelaxation method. We may wonder about the upper-bound for this accuracy from Equation 19; it can be shown that this is close to $5\delta_n$ (all the actual accuracies are much smaller than this). Another feature of interest worth pointing out is that the number of iterations n required in the simple relaxation method can be given by $(\log[\delta_n/\delta_0] \div \log[r_1 = \sqrt{0.97}])$, except where the sizes of the mirrors were reduced and thus losses over the normal transmissive ones were added. This is as we expect from Equation 13. Zernike(n,l) polynomials[15] were used to describe defects in the last two examples. These normalized polynomials $Z_n^l(\rho, \theta)$ are defined over the unit circle and hence, at each grid point (x, y) on the mirror of radius r, we define $\rho = (\sqrt{x^2 + y^2})/r$. We scale the amplitudes of the polynomials by 3×10^{-3} the wavelength of light (5.14×10^{-7} m), in keeping with the observed real mirror defects and the paraxial approximation.

V. Summary

We have presented and analyzed the numerical method based on FFT propagation discussed by Vinet and Hello[9], and demonstrated a method to reduce the time required by a large factor without losing any accuracy in the computed results. We have also indicated why such speed may be necessary — the numerical method can then be incorporated in a design environment that offers the user great flexibility in exploring his parameter space, or be used in more complicated coupled cavity systems without exorbitant demands on the processing time. Another aspect of our work was to present a way of tying the level of approximation to an upper-bound for the error in the results defined on the estimated field. In other words, once the designer knows to what accuracy he wants to compute a certain quantity, he can figure out what level of approximation (i.e. δ) and hence how much time he needs for his run. We anticipate that future papers will show the incorporation of this technique in the optical design of a full scale gravitational wave detector.

Acknowledgments

We thank Drs. J-Y Vinet and P. Hello, members of the VIRGO group, for generously donating their code for our use, and Dr. David Shoemaker for mediating the dialogue with them. A great deal of gratitude is owed to Prof. Rainer Weiss and Dr. Yaron Hefetz for their meticulous explanation of cavity physics that formed the basis for this work. Thanks are also due to Drs. David Shoemaker and Peter Fritschel, and Prof. Rainer Weiss for carefully reading the manuscript and suggesting appropriate changes.

This work was supported by the National Science Foundation cooperative agreement # PHY-9210038; the use of the Connection Machine 5 was through a grant of HPC time from the Project SCOUT at MIT-LCS, sponsored under ARPA contract # MDA972-92-J-1032.

References

1. A. E. Siegman, *Lasers* (University Science, Mill Valley, Calif., 1986), Chaps. 16—19.

2. A. G. Fox and T. Li, Computation of optical resonator modes by the method of resonance excitation, IEEE J. Quantum Electron. **QE-4**, 460—465 (1968).

3. L. Bergstein and H. Schachter, Resonant modes of optic cavities of small Fresnel numbers, J. Opt. Soc. Am. **55**, 1226—1233 (1965).

4. E. A. Sziklas and A. E. Siegman, Diffraction calculations using Fast Fourier Transform methods, Proc. IEEE **60**, 410—412 (1974).

5. M. M. Johnson, Direct application of the Fast Fourier Transform to open resonator calculations, Appl. Opt. **13**, 2326—2328 (1974).

6. R. Weiss, Electromagnetically coupled broadband gravitational antenna, MIT RLE Quarterly Progress Report **105**, 54—76 (1972).

7. A. Abramovici, *et. al.*, LIGO: The Laser Interferometer Gravitational-Wave Observatory, Science **256**, 325—333 (1992).

8. C. Bradaschia, *et. al.*, Interferometric detection of gravitational waves: the VIRGO project, *Gravitational Astronomy: Instrument Design and Astrophysical Prospects*, D. E. McClelland and H. A. Bachor, eds. (World Scientific, Singapore, 1991), pp. 110—135.

9. J. Vinet, P. Hello, C. N. Man, and A. Brillet, A high accuracy method for the simulation of non-ideal optical cavities, J. Phys. I France **2**, 1287—1303 (1992).

10. A. J. Trigdell, D. E. McClelland, and C. M. Savage, Numerially modeling a dual recycling Interferometric Gravitational Wave Detector, *Gravitational Astronomy: Instrument Design and Astrophysical Prospects*, D. E. McClelland and H. A. Bachor, eds. (World Scientific, Singapore, 1991), pp. 222—247.

11. The Connection Machine 5 (CM-5) is manufactured by Thinking Machines Corporation, 245 First Street, Cambridge, MA 02142.

12. W. H. Press, S. A. Teukolsky, W. T. Vetterling, B. P. Flannery, *Numerical Recipes in Fortran* (Cambridge University Press, New York, N.Y., 1992), pp. 395—398.

13. —, *ibid.*, pp. 854—860.

14. Thinking Machines Corporation, CMSSL for CM Fortran, Version 3.2.

15. R. J. Noll, Zernike polynomials and atmospheric turbulence, J. Opt. Soc. Am. **66**, 207—211 (1976).

List of Figures

The nominal parameters of the ideal cavity are as follows:
Length = 4000 m;
Front mirror: flat, diameter = 25 cm, power reflectivity = 0.97, no thickness;
Back mirror: curved, diameter = 25 cm, radius of curvature = 6000 m, reflectivity = 1;
External beam: Hermite Gaussian (0,0) mode of the ideal cavity; wavelength, $\lambda = 5.14 \times 10^{-7}$ m.

Type of defect	(Simple Relaxation, Overrelaxation)			
	δ_0	final $\delta_n(10^{-5})$	number of iterations	Accuracy(10^{-5})
Front mirror tilted 0.1 μrad	(0.29, 0.29)	(9.92, 7.53)	(525, 3)	(1.1, 1.2)
Back mirror tilted 0.1 μrad	(0.48, 0.48)	(9.96, 7.71)	(558, 4)	(1.7, 1.3)
Front mirror radius reduced 60%	(0.03, 0.03)	(9.93, 7.89)	(187, 15)	(2.2, 0.5)
Back mirror radius reduced 40%	(0.17, 0.17)	(9.98, 5.43)	(155, 14)	(5.3, 0.3)
Radius of curvature reduced 5%	(0.71, 0.71)	(9.89, 8.94)	(584, 8)	(2.3, 1.0)
$f(x,y) = 3 \times 10^{-3} \cdot \lambda \cdot$Zernike(6,0)	(0.09, 0.09)	(9.93, 9.01)	(453, 5)	(0.5, 0.9)
$b(x,y) = 3 \times 10^{-3} \cdot \lambda \cdot$Zernike(6,0)	(0.21, 0.21)	(9.87, 9.48)	(505, 25)	(0.7, 2.2)

Table 1: Examples comparing the two convergence techniques. δ_0 are the starting "amplitudes" of the "error" field, final δ_n show where we decide to stop the convergence. The first number within each pair of parentheses shows what we obtain with the simple relaxation method, the second one indicates the corresponding number for the overrelaxation scheme. Accuracy is the amplitude of the error field divided by the amplitude of a near exact (approximated with a δ_n of 10^{-8}) solution.

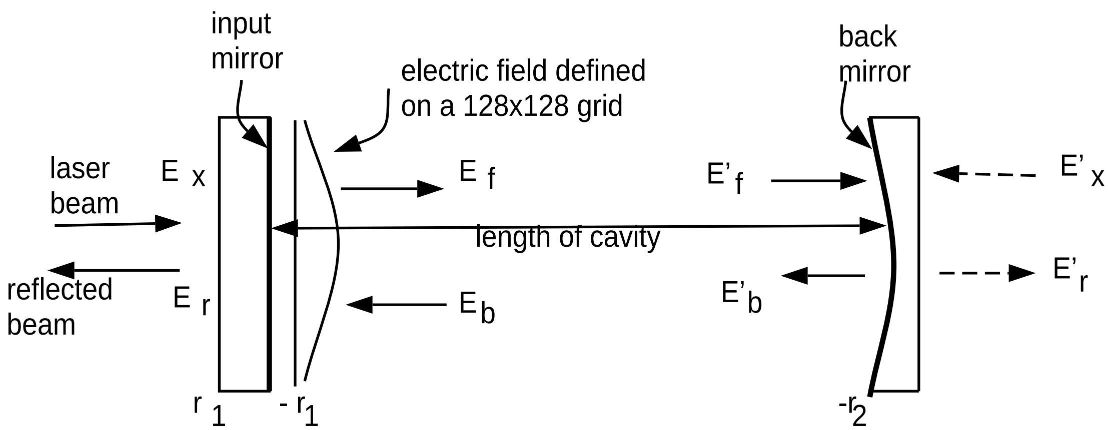
input
mirror
electric field defined
on a 128x128 grid
back
mirror
laser
beam
E x
E f
E' f
E' x
length of cavity
reflected
beam
E r
E b
E' b
E' r
r 1
- r1
-r2

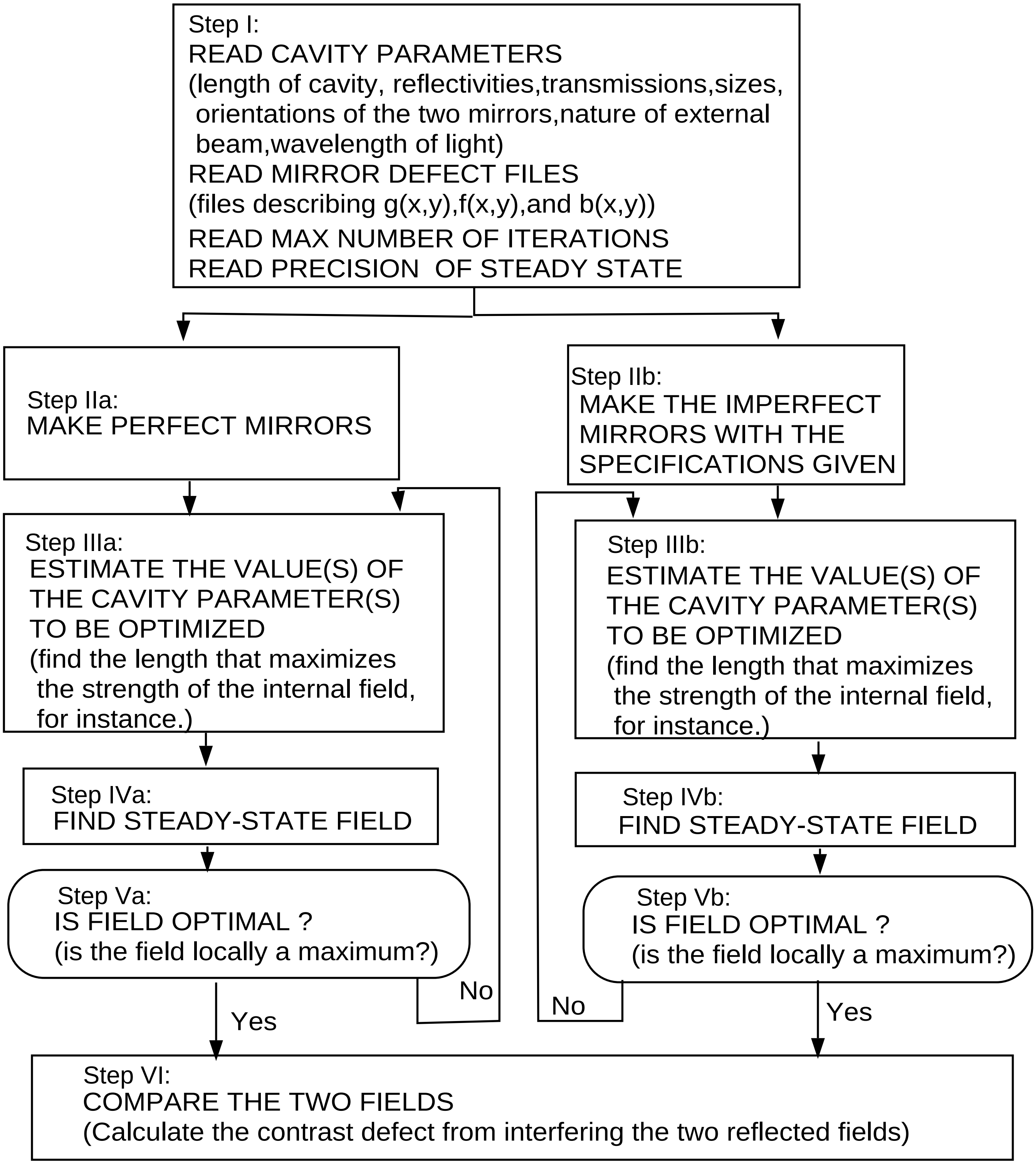
Step I:
READ CAVITY PARAMETERS
(length of cavity, reflectivities,transmissions,sizes, orientations of the two mirrors,nature of external beam,wavelength of light)
READ MIRROR DEFECT FILES
(files describing g(x,y),f(x,y),and b(x,y))
READ MAX NUMBER OF ITERATIONS
READ PRECISION OF STEADY STATE
Step IIa:
MAKE PERFECT MIRRORS
Step IIb:
MAKE THE IMPERFECT MIRRORS WITH THE SPECIFICATIONS GIVEN
Step IIIa:
ESTIMATE THE VALUE(S) OF THE CAVITY PARAMETER(S) TO BE OPTIMIZED
(find the length that maximizes the strength of the internal field, for instance.)
Step IIIb:
ESTIMATE THE VALUE(S) OF THE CAVITY PARAMETER(S) TO BE OPTIMIZED
(find the length that maximizes the strength of the internal field, for instance.)
Step IVa:
FIND STEADY-STATE FIELD
Step IVb:
FIND STEADY-STATE FIELD
Step Va:
IS FIELD OPTIMAL ?
(is the field locally a maximum?)
Step Vb:
IS FIELD OPTIMAL ?
(is the field locally a maximum?)
No
Yes
No
Yes
Step VI:
COMPARE THE TWO FIELDS
(Calculate the contrast defect from interfering the two reflected fields)

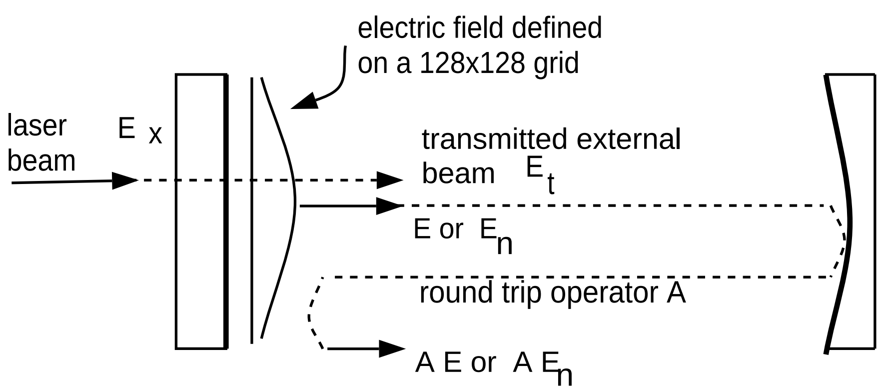

electric field defined
on a 128x128 grid
laser
beam
E x
transmitted external
beam E t
E or E n
round trip operator A
A E or A E n

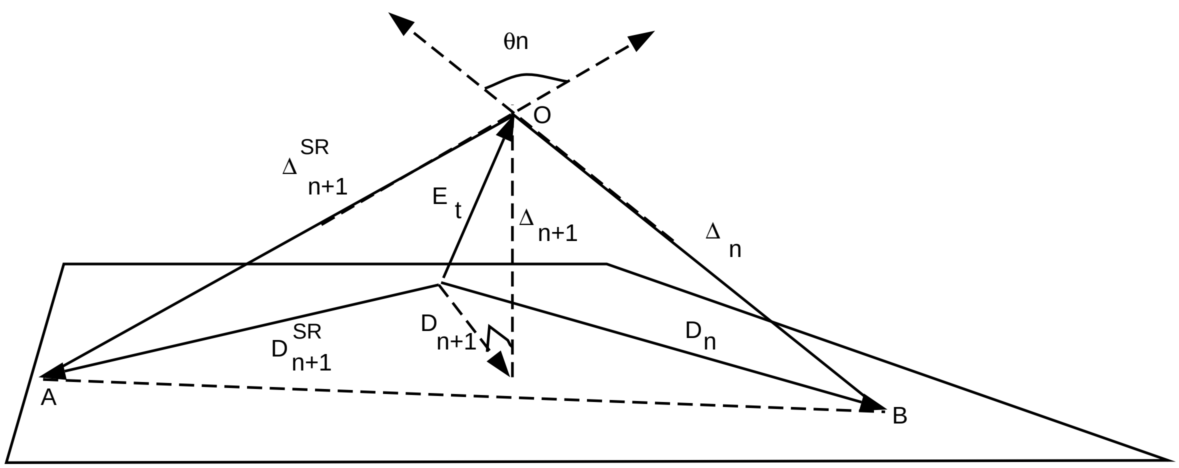
θn
O
Δ SR n+1
E t
Δ n+1
Δ n
D SR n+1
D n+1
D n
A
B